NASA

Technical Memorandum **79568**

Remote Sensing of Atmospheric Water Vapor, Liquid Water and Wind Speed at the Ocean Surface by Passive Microwave Techniques from the Nimbus-5 Satellite

A. T. C. Chang and T. T. Wilheit

JUNE 1977

National Aeronautics and
Space Administration

Goddard Space Flight Center
Greenbelt, Maryland 20771

REMOTE SENSING OF ATMOSPHERIC WATER VAPOR, LIQUID WATER AND WIND SPEED AT THE OCEAN SURFACE BY PASSIVE MICROWAVE TECHNIQUES FROM THE NIMBUS-5 SATELLITE

by

A. T C. Chang and T. T. Wilheit

June 1978

ABSTRACT

The microwave brightness temperature measurements for Nimbus-5 Electrically Scanned Microwave Radiometer (ESMR), and Nimbus E Microwave Spectrometer (NEMS) are used to retrieve the atmospheric water vapor, liquid water and wind speed by a quasi-statistical retrieval technique. It is shown that the brightness temperature can be utilized to yield these parameters under various weather conditions. Observations at 19.35 GHz, 22.235 GHz and 31.4 GHz were input to the regression equations. The retrieved values of these parameters for portions of two Nimbus-5 orbits are presented. Then comparison between the retrieved parameters and the available observations on the total water vapor content and the surface wind speed are made. The estimated errors for retrieval are approximately 0.15 g/cm^2 for water vapor content, 6.5 mg/cm^2 for liquid water content and 6.6 m/sec for surface wind speed.

CONTENTS

		Page
I.	Introduction	1
II.	Microwave Radiative Transfer in Atmosphere	2
III.	Quasi-Statistical Retrieval Technique	8
IV.	Results	13
V.	Conclusion	15

1. Introduction

In this paper we will discuss techniques for measuring the water vapor and liquid water content of marine atmospheres and the wind speed at the oceans surface. Using microwave remote sensing the importance of water vapor and wind speed measurements are well known and obvious. However, the liquid water content of the atmosphere has not been routinely measured and thus its relative importance is not firmly established. It is, nevertheless, available as a by-product of the remote sensing approach discussed in this paper and may well prove useful.

This remote sensing approach involves the measurement of emitted microwave radiation at several wavelengths and sorting out the various contributions to the measured brightness temperature. In a recent paper by Wilheit and Fowler (1977), a linear approximation method is used to analyze the wind speed and cloud liquid water content from a set of microwave measurements collected by an aircraft platform. Their data set was taken under a rather narrow range of subarctic conditions which permitted use of a simpler interpretation technique than is used here. In order to describe the techniques involved, we will first review the relevant aspects of microwave radiative transfer. We will then develop a statistical technique for retrieval of geophysical parameters from the measurements. Using this statistical technique, a data set involving observations over a typhoon in the Pacific Ocean will then be analyzed.

The specific sensors applied here are the Nimbus E Microwave Spectrometer (NEMS) and the Electrically scanned microwave Radiometer (ESMR), both of which are in orbit aboard the Nimbus-5 satellite. Detailed descriptions of these instruments can be found in Wilheit (1972) and Staelin et al (1972). For present purposes it is sufficient to note that the ESMR is a scanning instrument which measures the upwelling microwave radiation at 19.35 GHz while scanning 50° to either side of the spacecraft and has a spatial resolution of 25 km at nadir. The NEMS instrument views only at the nadir, and obtains observations at 22.235, 31.4 GHz and at three frequencies in the 50-70 GHz molecular Oxygen band (not of interest in this paper). It has a spatial resolution of 200 km.

A. Microwave Radiative Transfer in Atmosphere

In the microwave portion of the electromagnetic spectrum and at temperatures typical of the Earth and its atmosphere, the Rayleigh-Jeans approximation for black body radiation works quite well. This enables radiative transfer for an isotropic, nonscattering, nonreflecting medium to be expressed as follows:

$$\frac{dT_B}{dx} = -\alpha(T_B - T_o). \tag{1}$$

where T_B represents the intensity of radiation at a given wavelength and in the x direction expressed as an equivalent black body temperature, called brightness temperature. α is the absorption coefficient and T_o is the thermodynamic temperature of the medium. If this is integrated for a uniform slab of thickness, a, along the direction of propagation, x, the result becomes,

$$T_{B_{out}} = T_{B_{in}} e^{-\alpha a} + (1 - e^{-\alpha a}) T_o , \qquad (2)$$

where $T_{B_{in}}$ is the brightness temperature incident on the slab and $T_{B_{out}}$ represents the emerging brightness temperature.

If the expression, αa, is quite small or if $T_o - T_B$ is small, the slab has a very small effect on the intensity of the radiation; whereas, if the slab is opaque ($\alpha a \rightarrow \infty$) the radiation emerging out of the slab is characterized by the thermodynamic temperature of the slab independent of the intensity of the incident radiation. In this study, the atmosphere is divided into 100 layers each 0.2 km thick. Each layer is characterized by the temperature, pressure and concentration of constituents of the center of the slab. In a manner analogous to equation 1, the brightness temperature, T_B radiating from a surface is given by

$$T_B = (1 - e) T_{B_{Inc}} + e T_o . \qquad (3)$$

$T_{B_{Inc}}$ is the brightness temperature incident on the surface, e is the emissivity of the surface and T_o is the thermodynamic temperature of the surface. The incident energy must also be averaged appropriately over all angles which can be reflected into the viewing direction. Since most natural surfaces are quite rough when considered on the scale of microwave wavelengths (0.1 - 30 cm), we will use the Lambertian approximation (Born and Wolf, 1975) for this angular distribution.

$$T_{B_{Inc}} = 2 \int_o^{\pi/2} T_B(\theta) \cos\theta \sin\theta \, d\theta , \qquad (4)$$

where $T_B(\theta)$ is the incident brightness as a function of the incidence angle θ.

For computational simplicity, since the weighting function. (Sin θ cos θ) within the integrand has a maximum at $\theta = 45^{\circ}$, we will approximate $T_{B_{Inc}}$ by

$$T_{B_{Inc}} \cong T_B(\theta = 45^{\circ}). \tag{5}$$

Thus, to determine this brightness temperature which would be observed in a particular situation, we must be able to characterize the emissivity of the underlying surface and the absorption coefficient of the atmosphere as a function of their physical and chemical parameters.

The emissivity of terrestrial surfaces in the microwave region of the electromagnetic spectrum varies from 0.95 for most solid surfaces to about 0.4 for the ocean surface. It is this low emissivity and relative homogeneity of the calm ocean surface which provides the possibility of sounding the water vapor and liquid water content of the atmosphere.

The emissivity of a smooth ocean surface can be calculated from the dielectric constant through the Fresnel relations (Jackson, 1962). The dielectric constant data used here are from Lane and Saxton (1952). At a given frequency, v, the real part of the dielectric constant, ϵ', may be expressed as,

$$\epsilon' = \epsilon_\infty + (\epsilon_s - \epsilon_\infty)/(1 + \omega^2 \tau^2), \tag{6}$$

and the imaginary part, ϵ'', as,

$$\epsilon'' = \omega\tau(\epsilon_s - \epsilon_\infty)/(1 + \omega^2 \tau^2) + \sigma/\omega, \tag{7}$$

where $\omega = 2\pi v$. The ϵ_∞, ϵ_s, σ and τ values at a number of temperatures and NaCl concentration are given by Saxton and Lane (1952). And conductivity value as a function of temperature from the International Critical Tables (1928). These can be summarized by the analytical expressions

$$\epsilon_\infty = 4.9, \tag{8}$$

$$\epsilon_s = 190.0 - 81.0N + 38.0N^2 - (3.75 - 2N + N^2)\frac{T}{10.0}, \quad (9)$$

$$\tau = \frac{0.00199}{T} e^{\frac{2140}{T}} + \left[\frac{0.00972}{T} e^{\frac{2060}{T}} - \frac{0.00324}{T} e^{\frac{1968}{T}} - \frac{0.00597}{T} e^{\frac{2140}{T}}\right] N$$

$$+ \left[\frac{0.00648}{T} e^{\frac{1968}{T}} - \frac{0.00972}{T} e^{\frac{2060}{T}} + \frac{0.00398}{T} e^{\frac{2140}{T}}\right] N^2, \quad (10)$$

$$\sigma = 92.13N - 8.73N^2 + 3.12\,(T - 273)N - 0.37\,(T - 273)N^2. \quad (11)$$

T is the temperature in Kelvin and N the NaCl concentration in gram normal. The form used for the temperature dependence of τ was suggested on theoretical grounds by Saxton and appears necessary in light of the large temperature dependence of this particular parameter. The simple polynomial fit appears adequate for the remainder of these expressions. We will approximate sea water as a 0.6N NaCl solution.

When the sea surface is roughened by wind the situation becomes more complicated. Calculations by Stogryn (1967) indicate that there is little effect due to roughness for viewing at nadir. In horizontal polarization from nadir the roughness increases the emissivity and the effect increases with viewing angle out to at least 60°. In vertical polarization the roughness decreases the emissivity out to about 55° incidence angle, above which the emissivity increases with roughness and viewing angle. The observations of Hollinger (1970) only partially confirm the theoretical expectations but both agree that there is little or no effect due to roughness for viewing directly at nadir which is the case considered here.

In addition to roughening the sea surface; the wind also creates foam which can also increase the emissivity of the surface. Nordberg et al (1971) found that for a frequency of 19.35 GHz the foam coverage increases the emissivity

at nadir by 4.3×10^{-3} for each meter per second the wind speed exceeded 7 m/sec with no effect at wind speeds below 7 m/sec. Measurements have been made by Van Melle et al. (1973) at 2.69 GHz on an artificially generated foam; found an effect comparable to that of Nordberg et al. (1971). More recently Webster et al (1976) have measured the net effect of wind on the surface emissivity at several frequencies from 1.4 to 37 GHz at view angles of 0° (nadir) and 38°. They found little frequency dependence above 10 GHz and a somewhat weaker effect than found by Nordberg et al. On this basis we will in this paper assume that for the frequencies of present interest (19.35, 22.235, and 31.4 GHz) that each meter per second that the wind speed exceeds 7 m/s increases the surface emissivity by 3.2×10^{-3}. The determination of the effect of wind speed on surface emissivity as a function of frequencies, polarization and view angle remains an important research problem.

In the Earth's atmosphere at frequencies between 1 and 100 GHz only three constituents need to be considered: water vapor, liquid water and molecular oxygen. All other constituents normally found in the atmosphere have either a sufficiently low abundance or weak microwave absorption that they are ignorable. We will therefore consider only these three constituents. We will restrict this treatment also to non-raining situations to simplify the treatment of liquid water in atmosphere.

Water vapor has transitions at 22.235 GHz and 183.3 GHz in addition to many transitions at higher frequencies. Using the treatment given by Gaut (1968) the absorption coefficient can be expressed as:

$$\alpha = \alpha_{RES} + \alpha_{NON} \tag{12}$$

where α_{RES} refers to the contribution due to 22.235 GHz absorption line and can be written as:

$$\alpha_{RES} = \frac{343 \nu^2 \Delta\nu \rho}{T^{5/2}} e^{-644/T} \left[\frac{1}{(\nu - 22.235)^2 + \Delta\nu^2} + \frac{1}{(\nu + 22.235)^2 + \Delta\nu^2} \right], \quad (13)$$

where

$$\Delta\nu = \frac{0.126p \left(1 + 0.011 \frac{\rho T}{p}\right)}{T}$$

is the line width of the 22.235 GHz absorption line.

ρ = water vapor density, in g/m^3

P = Pressure, in Torr

T = temperature, in Kelvins

ν = propagating frequenty, in GHz

α_{NON} refers to the contribution from all other lines and can be written as,

$$\alpha_{NON} = 2.55 \times 10^{-3} \frac{\nu^2 \rho \Delta\nu}{T^{3/2}} . \quad (14)$$

For liquid water, as already noted, only non-precipitating clouds are considered in this study. Since in such clouds the typical particle size is much smaller than the wavelength of interest, the Rayleigh approximation (Gunn and East, 1954) should be quite adequate to represent the scattering by cloud particles less than 100 micron. The absorption coefficient can be written as:

$$\gamma_{Cloud}\,(km^{-1}) = \frac{0.188\, m\, \epsilon''}{(\epsilon' + 2)^2 + (\epsilon'')^2} \quad (15)$$

where m = cloud liquid water content of atmosphere, in gm/m^3.

The dielectric data (ϵ' and ϵ'') used are those of Lane and Saxton (1952) and discussed in the previous paragraph for the special case of pure water. The

combination of the factor of ν in this expression of ϵ' and ϵ'' results in a frequency dependence of approximately ν^2 for the absorption coefficient of clouds. Since clouds are often supercooled below the 265 K lower temperature limit of the Lane and Saxton dielectric data on which an expression for ϵ' and ϵ'' are based, it is important that we have chosen an expression for the relaxation time, τ which has some theoretical foundation.

The absorption by the complex of molecular oxygen resonances near 0.5 cm can be approximated for frequencies below 45 GHz by treating them as a line with a resonant term and a non-resonant term. The absorption coefficient can be written as:

$$\alpha = \frac{0.3\,P}{T^2}\left\{\frac{\Delta\nu}{(\nu-\nu_o)^2+\Delta\nu^2}+\frac{\Delta\nu}{\nu^2+\Delta\nu^2}\right\} \tag{16}$$

where $\nu_o = 60$ GHz and $\Delta\nu$ is the pressure broadening in GHz.

$$\Delta\nu = \begin{cases} 7.91\times10^{-3}\,P\left(\frac{300}{T}\right)^{0.85} & P > 250 \text{ torr} \\ 1.55\times10^{-3}\,P\left(\frac{300}{T}\right)^{0.85}\left(\frac{231+0.49\,(19-P)}{231}\right) & 250 \geq P \geq 19 \text{ torr} \\ 1.55\times10^{-3}\,P\left(\frac{300}{T}\right)^{0.85} & P < 19 \text{ torr} \end{cases} \tag{17}$$

Calculations based on this approximation agree well with those based on full Meeks and Lilly (1963) expression as modified by Lenoir (1968) for frequencies less than 45 GHz.

III. Quasi-Statistical Retrieval Technique

As can be seen from the previous section, the brightness temperature which

would be observed upwelling from the atmosphere depends on many geophysical variables. However, several of the variables (temperature, humidity, and liquid water content) are, in themselves, continuous functions of height. Therefore, this problem has an infinite number of degrees of freedom. In the most general sense, a retrieval of geophysical variables from a finite set of observations could never be performed. We must resort to approximations and constrained sol tions if we are to derive useful information.

One technique for retrieving geophysical parameters is the statistical technique which was applied, quite successfully, by Waters et al (1975) to the problem of approximating the atmospheric temperature profile from microwave brightness temperature measurements in the molecular Oxygen band ($\lambda \simeq 5$ mm). In this technique, they begin with a statistical data base that consisted of a large set of actual tempe soundings. For each of these soundings, they calculate the expected upwelling brightness temperature at all frequencies at which measurements are to be made. The temperature at various heights are then regressed against the brightness temperature to determine the most probable (if the statistics are Gaussian) temperature from each level.

If there is little information about a given level in the brightness temperature, then the retrieved temperature will tend toward the a priori average of the statistical data set and the residual of the regression will be little smaller than the variance of the a priori data set. It is to be noted that information about a given level can occur in a given measurement both directly through the equation of radiative transfer and also indirectly through correlations inherent to the atmosphere itself.

This technique may be faulted in that it contains any bias of the a priori data

set. When the brightness temperatures are strongly related in a direct sense to the geophysical parameters being retrieved, this would be of little consequence, but where the coupling is through statistical correlations among the geophysical observables or when the retrieval offers only marginal improvement over the a priori statistics then the retrieved values will tend strongly toward the commonplace situations. This may well give average statistics which suggest a very good retrieval technique but which gives poor results in the extraordinary situation which is often of the most interest. We, therefore, have modified this technique somewhat. We generate an artificial data set subtending the entire expected range in all the geophysical variables at issue and force any correlations among them to be zero or at least much smaller than expected in nature. As a by-product, this relieves us the necessity of providing a true statistical data base for parameters which have been measured sparsely or not at all.

In the present case, we wish to interpret measurements made at frequencies of 19.35, 22.235, and 31.4 GHz. On the basis of the microwave properties of the atmosphere, we would expect the brightness temperature to be affected strongly by the wind speed at the sea surface and the net content of water vapor and liquid water in the atmosphere and rather weakly by sea surface temperature, cloud temperature and details of the vertical distribution of water vapor. Thus variables such as details of the temperature structure of the atmosphere would be expected to be quite significant. Thus for our statistical data base, we select values from handbook atmospheres (Air Force Cambridge Research Laboratory, 1965) each with its associated water vapor content as specified in Table 1. In

Table 2, we specify the values of sea surface temperature, and surface wind speed and in Table 3 we give the cloud models used. The statistical data base then consists of all possible combinations of these four parameters. This would provide zero correlation among the four parameters. However, we also specify that wherever the cloud liquid water content is not zero, the relative humidity must be 100% at that altitude. This gives a weak correlation between cloud liquid water content and net water vapor and provides some additional variability in the vertical distribution of water vapor. Thus, for the present case, at each of three frequencies we calculate brightness temperature for every possible combination, within our set of, sea surface wind, sea surface temperature, atmosphere model and cloud model. There are a total of 1296 data sets generated which contain the following information: sea surface wind; net water vapor content; net liquid water content; T_B (19.35 GHz); T_B (22.235 GHz); T_B (31.4 GHz). Conventional linear predictions can then be generated for each of the first three of these based on the last three while adding appropriate instrument noise to the brightness temperature from a random number generator. While the linear approach works reasonably well, the dependence of the brightness temperature on the atmospheric water components is not linear. Rather the optical depth is more nearly linearly related to the water components. If, for the moment, we treat the atmosphere as a single layer with an optical depth $\tau = \tau_{vapor} + \tau_{liquid}$ and a thermodynamic temperature t_1, while the surface reflectance is R and has a temperature t_2. We will also make the approximation

that $t_1 \approx t_2$ and we will ignore the cosmic background. Then the upwelling brightness T_B is given by:

$$T_B = (1 - R\, e^{-(1+\sqrt{2})\tau})\, t_1 \tag{18}$$

The $\sqrt{2}$ occurs because of the approximation to a Lambertian surface discussed earlier. The logarithmic form of equation 18 can be written as

$$\mathrm{Ln}(t_1 - T_B) = \mathrm{Ln}(Rt_1) - (1+\sqrt{2})\,\tau_{vapor} + (1+\sqrt{2})\,\tau_{liquid}. \tag{19}$$

We then note that the function $\mathrm{Ln}(t_1 - T_B)$ is linearly related to each of the components of atmospheric water. Since the 22.235 GHz and 31.4 GHz channels are primarily sensitive to water vapor and liquid water we will use these logarithmic functions rather than the brightness temperature for these two frequencies and use the brightness temperature itself at 19.35 GHz. This discussion is not at all rigorous, but it serves to describe the gross behavior of the relationships and the functions so derived will mitigate the non-linear behavior of the problem. Since we are dealing with brightness temperature much colder than the thermodynamic temperature of the surface or atmosphere, we are not particularly sensitive to the value chosen for t_1, thus for present purposes we will set $t_1 = 280$ K. We then solve for the three geophysical parameter wind speed (W), cloud liquid water content (L) and water vapor (P) by conventional linear regression so that the parameters are solved for in the form

$$\begin{pmatrix} W \\ L \\ P \end{pmatrix} = \begin{pmatrix} a_1 \\ a_2 \\ a_3 \end{pmatrix} + \begin{pmatrix} b_{11} & b_{12} & b_{13} \\ b_{21} & b_{22} & b_{23} \\ b_{31} & b_{32} & b_{33} \end{pmatrix} \begin{pmatrix} T_{B_{19.35}} \\ \mathrm{Ln}(280 - T_{B_{22}}) \\ \mathrm{Ln}(280 - T_{B_{31}}) \end{pmatrix} \tag{20}$$

where the values of the a's and b's are given in table 4. In table 4 we also give the residual of each of the regressions which serves as an estimate the accuracy with which the retrieval can be made and the a priori standard deviation of each of the variables which specifies the variability in the data base.

IV. Results

To demonstrate the retrieval technique, two orbits of Nimbus 5 ESMR and NEMS data were chosen. In order to utilize both ESMR and NEMS data for the retrieval calculations, these data must be matched up geographically. Since the instantaneous field of view (IFOV) for the NEMS radiometers are quite different from that of ESMR, it is necessary to sum up all the 25 km × 25 km ESMR IFOV's which are contained within the NEMS' IFOV that is approximately 200 km × 200 km. The brightness temperatures measured at 0.96 cm, 1.35 cm and 1.55 cm radiometers for portions of orbits number 2891 and 2918 are shown in Figures 1 and 2 plotted as a function of latitude. These matched data sets were then input into equation 20 to yield the estimates of the surface wind speed, cloud liquid water content and water vapor content in the atmosphere. The results of these computations are also shown in Figures 1 and 2 along with the corresponding ESMR images. By showing rain and land areas as dark shades, a spatial perspective on the data is provided. The specific data sets used here are from Nimbus-5 orbits 2891 and 2918 which passed near the eye of Typhoon Billie at about 1500 Z on July 14 and 16, 1973 respectively. Figures 3 and 4 give the corresponding surface analyses (each three hours earlier than the satellite pass) along with relevant observations of wind speed and atmospheric water vapor content.

Examination of the water vapor retrievals shows first that this varies smoothly with little structure. More specifically, on July 14, it can be seen that the retrieved water vapor of about 4.5 cm at 30°N agrees almost exactly with the observations. Further, the slight decrease in water vapor along the track to about 25°N is also supported by the observations. Beyond that, there are no supporting water vapor observations for this orbit. On July 16 similar agreement is observed between water vapor observations and retrievals. There are no direct observations of cloud liquid water content but the areas with liquid water retrievals below 1 mg/cm correspond to clear areas as indicates by thermal infrared images from the same satellite. Also the fact that the bulk of the retrieved data are very near to 0 mg/cm suggests that there is no consequential bias in this retrieval. Examination of the wind speed observations shows most observations in the 15-30 kt (7.5-15 m/sec) range away from the storm center consistent with the retrievals and no observations in the high wind portions of the typhoon.

V. Conclusion

We have developed a quasi-statistical technique suitable for retrieval of geophysical parameters from microwave radiometric observations. We have derived specific equations for retrieving the wind speed at the oceans surface, and the atmospheric contents of both liquid and water vapor from simultaneous observations at 19.35 GHz, 22.235 GHz, and 31.4 GHz and applied these equations to data taken by the Nimbus-5 spacecraft and by comparing the results with available observations shown that the results are promising.

The estimates of liquid water content in this study could be biased upward in the presence of precipitation, because the present regression analysis is performed on the non-raining data ensemble. Further study in this area is required to resolve this problem.

References

1. Air Force Cambridge Research Laboratory, Handbook of Geophysics and Space Environments, McGraw Hill, New York, 1965.

2. Born, M. and E. Wolf: Principles of Optics, p. 182, Pergamon Press, Oxford, 1975.

3. Gaut, N. E.: Studies of Atmospheric Water Vapor by Means of Passive Microwave Techniques, Technical Report 437, Research Laboratory of Electronics, Massachusetts Institute of Technology, 1968.

4. Gunn, K. L. S. and T. W. R. East: The Microwave Properties of Precipitation Particles, Royal Meteorological Society, Vol. 80, pp 522-545, 1954.

5. Hollinger, J. P., Passive Microwave Measurements of Sea Surface Roughness, Trans. IEEE GE Vol 9, pp 165-169, 1971.

6. International Critical Tables of Numerical Data, Physics, Chemistry and Technology, Vol. IV, McGraw Hill, New York, pp 231-239, 1928.

7. Jackson, J. D.: Classical Electrodynamics, p. 219, John Wiley and Sons, Inc., New York, 1962.

8. Lane, J. A. and J. A. Saxton: Electrical Properties of Sea Water, Wireless Engineering, Vol. 29, pp 269-275, 1952.

9. Lenoir, W. B.: Microwave Spectrum of Molecular Oxygen in the Mesosphere, J. G. R., Vol. 73, pp 361-376, 1968.

10. Meeks and Lilly: The Microwave Spectrum of Oxygen in the Earth's Atmosphere, J. G. R., Vol. 68, pp 1683-1703, 1963.

11. Nordberg, W., J. Conaway, Duncan B. Ross and T. Wilheit: Measurements of Microwave Emission from a Foam-Covered, Wind-Driven Sea, J.A.S., Vol. 28, pp 429-435, 1971.

12. Saxon, J. A. and J. A. Lane: Dielectric Dispersion in Pure Polar Liquids at Very High Radio-Frequencies

I. Measurements on Water, Methyl and Ethyl Alcohols, Proc. Roy. Soc., Vol. 213, pp 400-408, 1952.

13. Staelin, D. H., F. T. Barath, J. C. Blinn III, and E. J. Johnson: The Nimbus E Microwave Spectrometer (NEMS) Experiment, Nimbus-5 User's Guide. NASA/GSFC Greenbelt, Maryland pp 141-157, 1972.

14. Stogryn: The Apparent Temperature of the Sea at Microwave Frequencies, Trans. IEEE Ant. and Prop. 15, pp 278-286, 1967.

15. Van Melle, M. J., H. H. Wang and W. F. Hall: Microwave Radiometers Observations of Simulated Sea Surface Conditions, JGR Vol. 78, 969, 1973.

16. Webster, W. J., Jr., T. T. Wilheit, D. B. Ross, and P. Gloersen: Spectral Characteristics of the Microwave Emission from a Wind Driven Foam-Covered Sea, JGR Vol 81 3095-3099, 1976.

17. Waters, J. W., K. F. Kunzi, R. L. Pettyjohn, R. K. L. Poon and D. H. Staelin: Remote Sensing of Atmospheric Temperature Profiles with Nimbus-5 Microwave Spectrometer, JAS, Vol. 32, pp 1953-1969, 1975.

18. Wilheit, T. T., The Electrically Scanning Microwave Radiometer (ESMR) Experiment: Nimbus-5 User's Guide, NASA/GSFC Greenbelt, Maryland pp 59-105, 1972.

19. Wilheit, T. T., and M. G. Fowler: Microwave Radiometric Determination of Wind Speed at the Surface of the Ocean During BESEX, Joint issue Trans IEEE AP Vol. 25 111-120, 1977 and Trans IEEE OE Vol. 2 111-120, 1977.

Table I

Handbook Atmosphere	Water Vapor Content (g/cm^2)
1. U. S. Standard	1.60
2. Tropical	3.88
3. Subtropical summer	4.23
4. Subtropical winter	2.12
5. Midlatitude summer	2.93
6. Midlatitude winter	0.87
7. Subarctic summer	2.07
8. Subarctic winter	0.42
9. Arctic winter	0.20

Table II

Sea Surface Temperature Values (k)	Surface Wind Speed Values (m/sec)
1. 273.0	1. 0
2. 283.0	2. 10
3. 293.0	3. 20
4. 303.0	4. 30

Table III

	Cloud Top (km)	Cloud Bottom (km)	Liquid water density (g/m^3)
1	2	1	0.01
2	2	1	0.2
3	8	7	0.01
4	8	7	0.2
5	6	1	0.01
6	6	1	0.2
7	8	6	0.01
8	8	6	0.2
9	No Cloud		

Table IV

Regression Coefficients

a_1	-1008.
a_2	1.831
a_3	37.92
b_{11}	2.330
b_{12}	66.81
b_{13}	76.68
b_{21}	-0.0024
b_{22}	-0.0146
b_{23}	-0.2941
b_{31}	-0.0479
b_{32}	-8.699
b_{33}	2.421

A Priori

	Mean	Standard Deviation	Estimated Error
(a) Water vapor content (g/cm^2)	2.35	1.64	0.15
(b) Liquid water content (g/cm^2)	0.019	0.030	0.0065
(c) Wind speed (m/sec)	15.	11.2	6.6

Figures

Figure 1. The measured brightness temperatures and the ESMR image of Nimbus 5 orbit no. 2891, July 14, 1973. The estimates of the water vapor content, the cloud liquid water content and the surface wind speed along the subsatellite track are presented.

Figure 2. The measured brightness temperatures and the ESMR image of Nimbus 5 orbit no. 2918, July 16, 1973. The estimates of the water vapor content, the cloud liquid water content and the surface wind speed along the subsatellite track are presented.

Figure 3. The surface weather chart corresponding to the studied area for 1200Z July 14, 1973. The percentage of relative humidity and water vapor content (g/cm^3) for several weather stations are shown for references.

Figure 4. The surface weather chart corresponding to the studied area for 1200Z, July 16, 1973. The percentage of relative humidity and water vapor content (g/cm^2) for several weather stations are shown for reference.

Tables

Table I. Handbook atmospheres used in this study and their corresponding water vapor contents.

Table II. The values of sea surface temperatures and surface wind speed used in this study.

Table III. The cloud models and their liquid water density used in this study.

Table IV. The regression coefficients for equation (20) and the residual of the regressions.

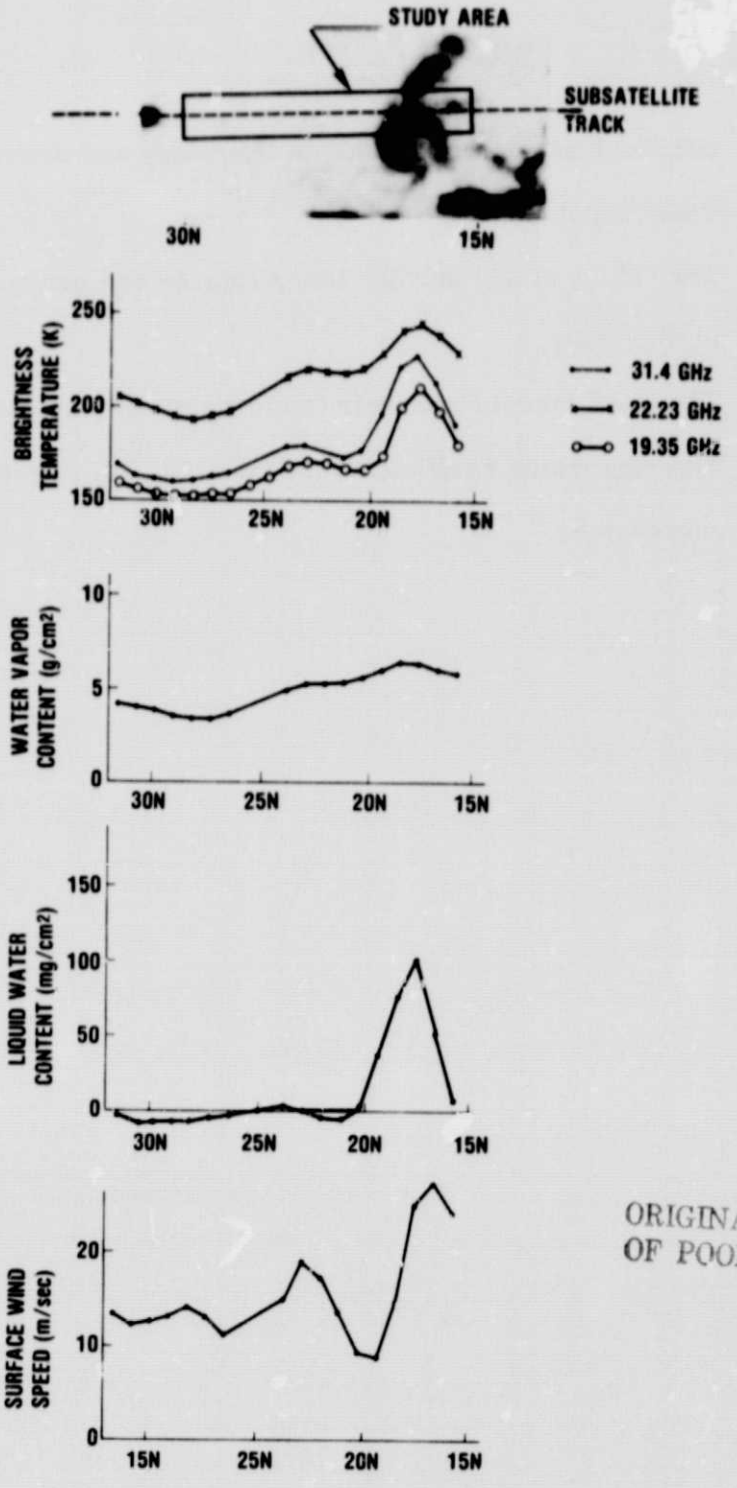

Figure 1. The measured brightness temperatures and the ESMR image of Nimbus 5 orbit no. 2891, July 14, 1973. The estimates of the water vapor content, the cloud liquid water content and the surface wind speed along the subsatellite track are presented.

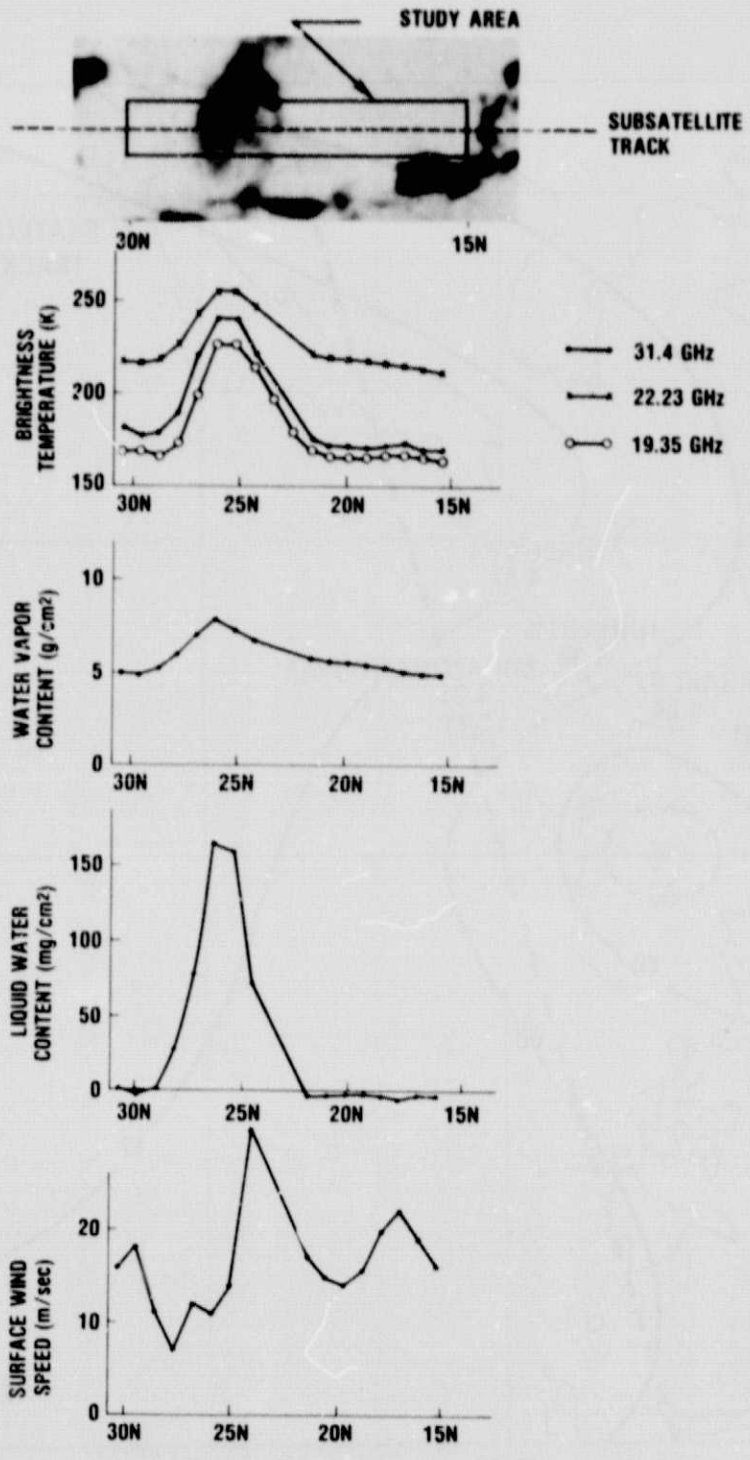

Figure 2. The measured brightness temperatures and the ESMR image of Nimbus 5 orbit no. 2918, July 16, 1973. The estimates of the water vapor content, the cloud liquid water content and the surface wind speed along the subsatellite track are presented.

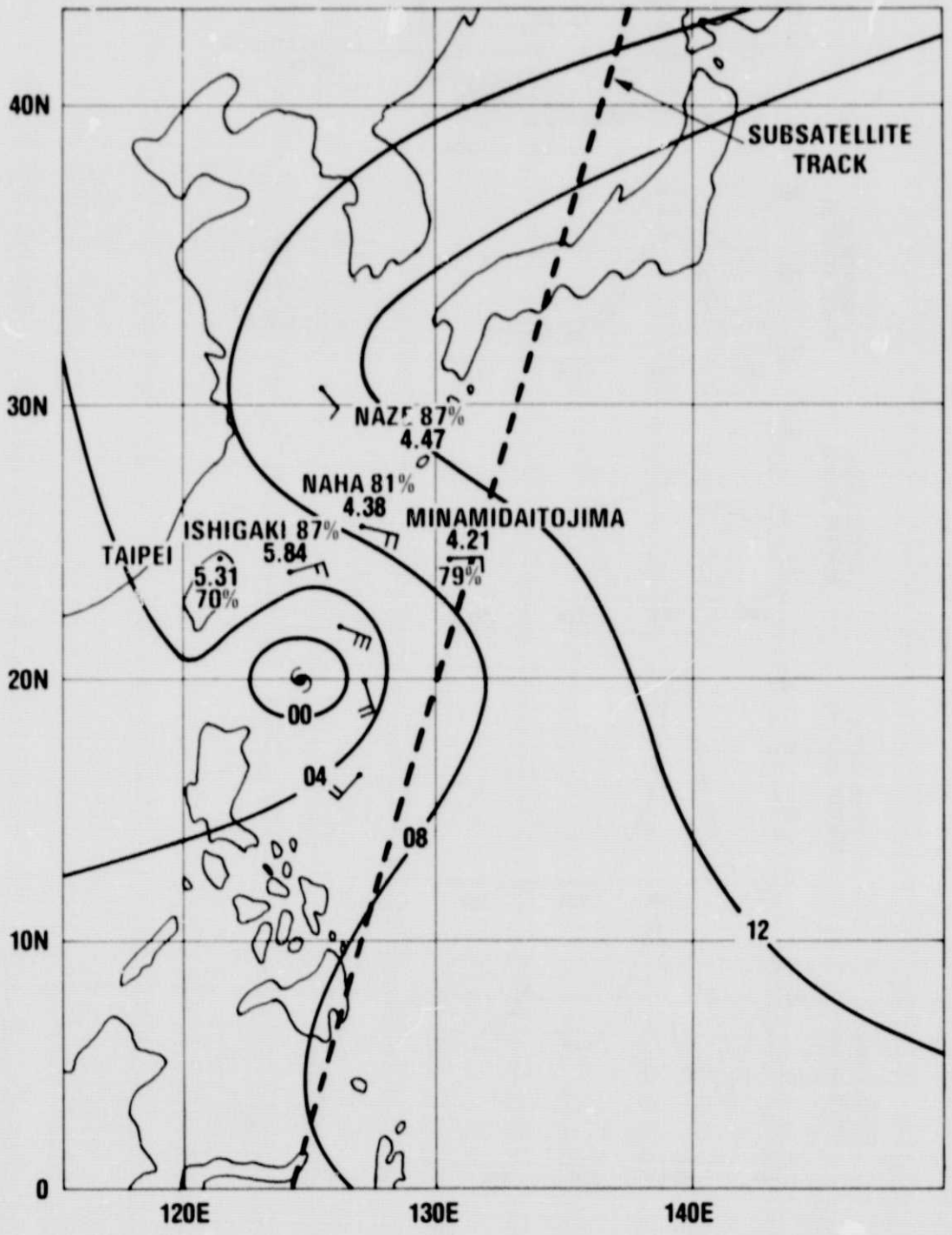

Figure 3. The surface weather chart corresponding to the studied area for 1200Z July 14, 1973. The percentage of relative humidity and water vapor content (g/cm^2) for several weather stations are shown for references.

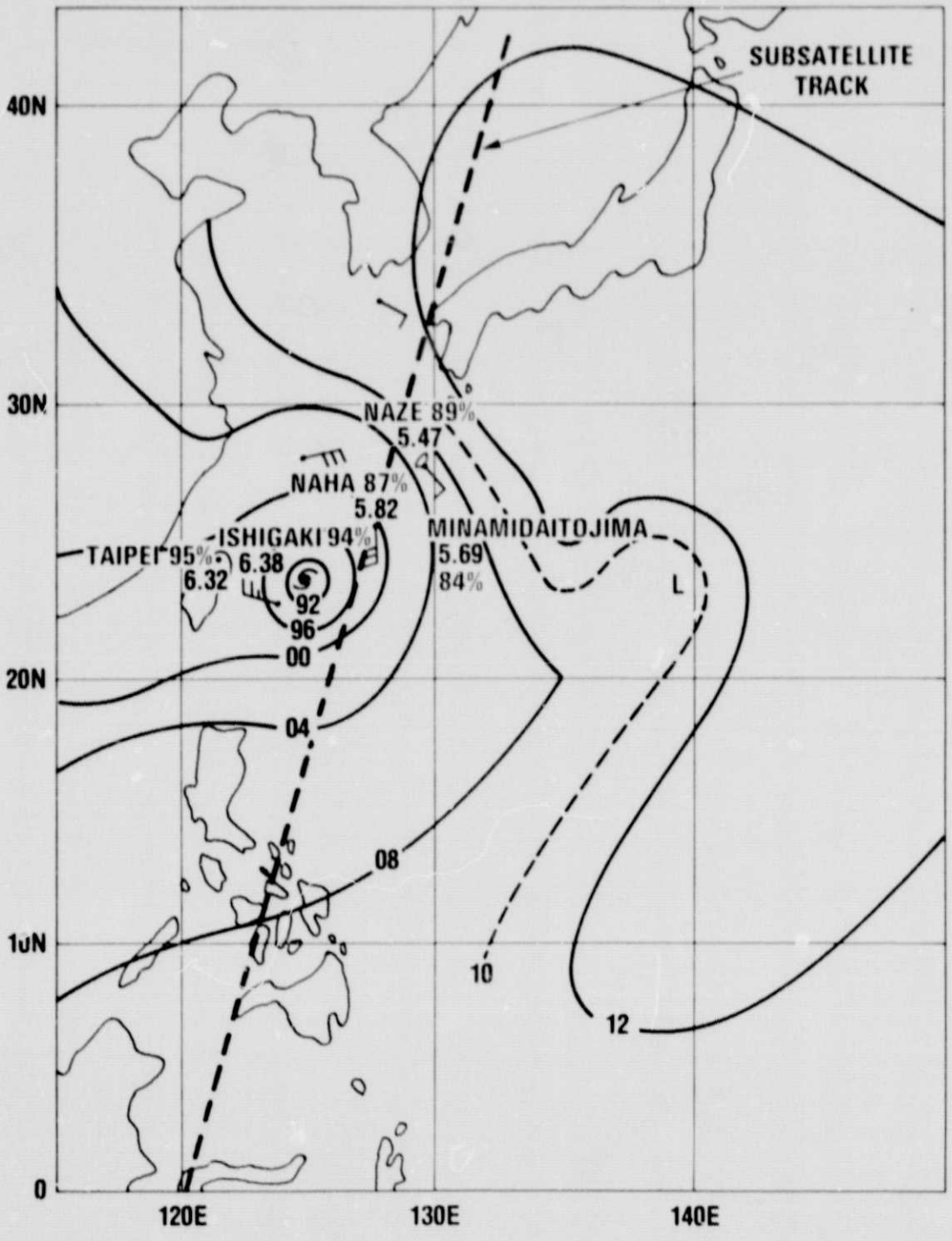

Figure 4. The surface weather chart corresponding to the studied area for 1200Z, July 16, 1973. The percentage of relative humidity and water vapor content (g/cm^2) for several weather stations are shown for reference.